ECS Transactions, 25 (2) 2753-2760 (2009)
10.1149/1.3205836 ©The Electrochemical Society

Oxygen Incorporation Reaction into Mixed Conducting Perovskites: A Mechanistic Analysis for (La,Sr)MnO_3 Based on DFT Calculations

Rotraut Merkle[a)], Yuri A. Mastrikov[b,c)], Eugene Heifets[a,b)], Eugene A. Kotomin[a,b)]
Maija Kukla[c)], Joachim Maier[a)]

[a)] Max-Planck Institute for Solid State Research
Heisenbergstr. 1, D-70569 Stuttgart, Germany
[b)] Institute for Solid State Physics, University of Latvia, Riga LV-1063, Latvia
[c)] Materials Science & Engineering Department, University of Maryland
College Park MD-20742-2115, USA

Based on DFT calculations of intermediates and transition states, several hypothetical mechanisms for oxygen incorporation into mixed conducting $La_{1-x}Sr_xMnO_{3\pm\delta}$ perovskites are discussed. In the most probable mechanism, the rate-determining step comprises the encounter of a highly mobile surface oxygen vacancy and a molecular oxygen adsorbate. Starting from these results, the variation of reaction rates for different materials is explored.

Introduction

Mixed conducting perovskites are applied as cathode materials in solid oxide fuel cells (SOFC) since the early 1980's, and $La_{1-x}Sr_xMnO_{3\pm\delta}$ was the first material from this class which found wide application. The fact that the ionic conductivity of these manganites is low (1,2) does not necessarily imply that the reaction is limited to the three-phase-boundary or that bulk transport becomes limiting. Under certain conditions the cathode process can also become limited by the oxygen incorporation surface reaction (2,3). The complete mechanism of the oxygen incorporation reaction at the perovskite surface cannot be resolved from experiments alone. On the one hand, this is due to the fact that the measurements (e.g. impedance spectroscopy (4)) yield only effective kinetic parameters. On the other hand, the application of surface sensitive techniques for the identification or even quantification of intermediate (adsorbate) species is limited by the requirement to work close to operation conditions, i.e. at elevated temperatures (typically 400 - 800 °C) and - most importantly - oxygen partial pressures at least in the mbar range instead of the typical UHV conditions. Thus first-principles atomistic DFT calculations can considerably contribute to the detailed understanding of the oxygen incorporation reaction.

Computational Details

The VASP 4.6.19 computer code (5) was used with Perdew-Wang 91 GGA nonlocal exchange-correlation functional and plane wave basis set (PW). Open shell Mn ions were treated with a spin-polarized approach. Effective charges on ions were calculated by the Bader (topological) analysis (6). Further computational details are given in Ref. (7). Under typical SOFC operation conditions (T = 1000 K, pO_2 = 0.2 to 1 bar), the most stable surface of $LaMnO_3$ is the MnO_2[001] termination. This conclusion was obtained from calculations of the surface Gibbs free energy for the different terminations (8,9).

The calculations of surface species were performed on symmetric 7-layer slabs $MnO_2(LaOMnO_2)_3$ which allows us to avoid the presence of a dipole moment on a polar surface, but has a Mn excess relative to La and an increased oxygen content. This slightly affects reaction enthalpies, e.g. for dissociative oxygen adsorption on the MnO_2[001] surface: $O_2 + 2\ Mn_{Mn}^{x} \rightarrow 2\ O_{ad}^{-} + 2\ Mn_{Mn}^{\bullet}$
which amounts to -2.7 eV for a stoichiometric $(LaOMnO_2)_4$ but asymmetrical 8-layer slab and -2.2 eV for the symmetrical $MnO_2(LaOMnO_2)_3$ slab (10). Since the symmetrical configuration has the advantage of identical surface layers and requires less computation time, all further calculations refer to the 7-layer slab. As the DFT calculations correspond to zero Kelvin, the $LaMnO_3$ slab adopts the orthorhombically distorted perovskite structure. For the calculation of adsorbates and surface defects a surface supercell corresponding to a coverage of 12.5 % was chosen. All concentrations (designated by square brackets) are given as the number of particles per surface or bulk unit cell comprising one $LaMnO_3$ formula unit. Reaction rates are calculated for T = 1000 K and pO_2 = 1 bar and expressed per surface unit cell (3.9 Å × 3.9 Å) and second.

Results and Discussion

As the starting point for the comparison of different mixed conducting perovskites we breifly summarize the results obtained for oxygen incorporation into $LaMnO_3$ (9). Figure 1a shows molecular and atomic oxygen adsorbates resulting from the interaction of an O_2 molecule with the defect-free MnO_2-terminated [001] surface of $LaMnO_3$. In contrast to oxygen interaction with large-bandgap oxides such as $SrTiO_3$ (11), already on the defect-free $LaMnO_3$ surface a strongly exothermic chemisorption occurs because the Mn ions can easily transfer electrons to adsorbates. The molecular adsorbates show in Fig. 1a can be assigned as superoxide O_2^- and peroxide O_2^{2-} based on their Bader charges (compare -1.25 e_0 for bulk oxide ions) and O-O bond lengths (compare 1.30 Å for gaseous O_2). The adsorbed atomic species corresponds to O^-.

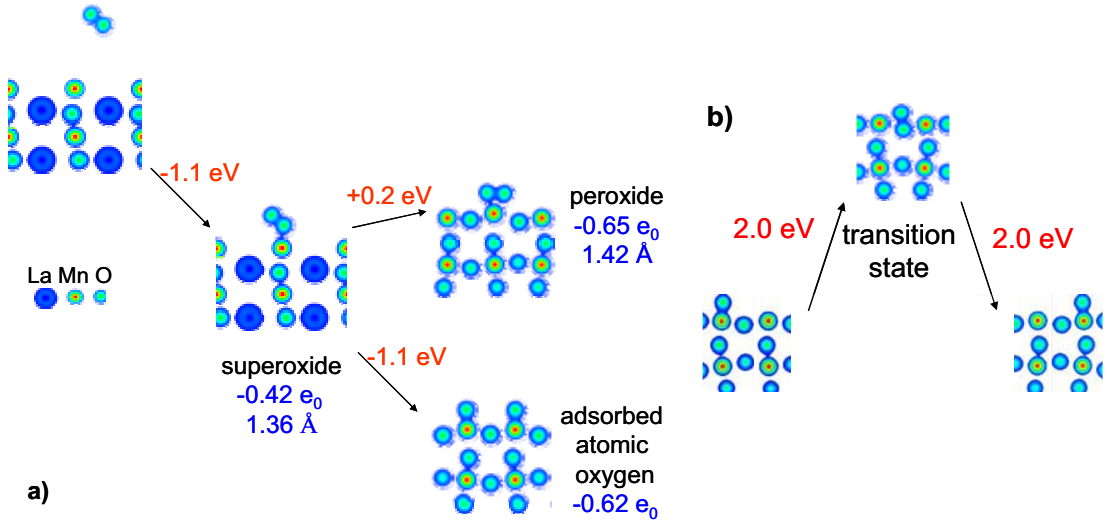

Figure 1. a) Molecular and dissociative oxygen adsorption on the MnO_2[001]-terminated $LaMnO_3$ surface. Bader atomic charges and O-O bond lengths of the adsorbates are indicated. b) Diffusion of adsorbed O^- along the MnO_2-terminated [001] surface. The transition state with the adsorbed O^- atop a lattice oxygen ion can also be regarded as a peroxide ion O_2^{2-} adsorbed into a surface oxygen vacancy.

Although these oxygen adsorption reactions are strongly exothermic, the adsorbate concentrations are expected to be low. This is due to the negative adsorption entropy in combination with the electrostatic repulsion between the adsorbates which leads to a flattening of the isotherms as soon as the coverage θ reaches the percent range (see Figure 2). The isotherms of the minority adsorbates O_2^- and O_2^{2-} flatten for $pO_2 > 10^{-4}$ bar because they feel the repulsion from the dominating O^- species.

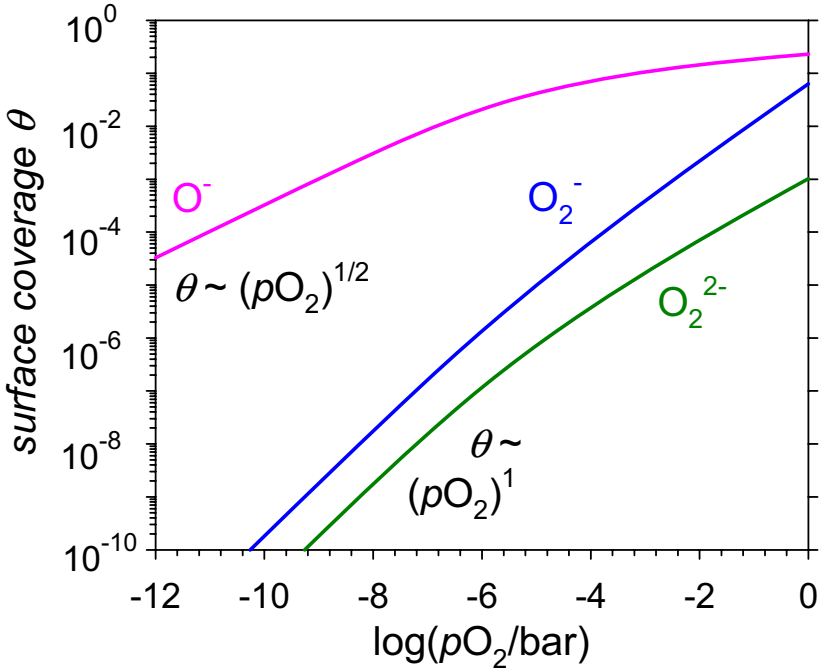

Figure 2. Oxygen chemisorption isotherms for 1000 K derived from DFT-calculated adsorption enthalpies (ΔH^0_{ad} = -1.1 eV for O_2^-, -0.9 eV for O_2^{2-}, -2.2 eV for 2 O^-) and adsorption entropies amounting to 50 - 80 % of the experimental entropy of O_2 at 1000 K (ΔS^0_{ad} = - 120 J/mol K for O_2^- and O_2^{2-}, -200 J/mol K for O^-). For details see Refs. (9,12).

For the discussion of various hypothetical oxygen incorporation reaction mechanisms, the oxygen vacancy concentration in the bulk and particularly in the surface layer also has to be known. For the actual use as SOFC cathode material, not the undoped $LaMnO_{3\pm\delta}$ is applied, but strontium-doped compositions $(La,Sr)(Mn)O_{3-\delta}$ which are brought into the slightly oxygen deficient regime by the acceptor doping. The bulk oxygen vacancy concentration typically amounts to $[V_O^{\cdot\cdot}] \approx 10^{-9}$ for $La_{0.8}Sr_{0.2}MnO_{3-\delta}$ at 700 °C and pO_2 = 1 bar (13). The oxygen vacancy formation enthalpy $\Delta H_{V_O^{\cdot\cdot}}$ is less endothermic by about 1 eV at the MnO_2[001]-terminated surface (10). At 700 °C, this leads to an enhancement of the vacancy concentration in the surface layer by a factor of 10^5. The migration activation energy of $V_O^{\cdot\cdot}$ is reduced to 0.67 eV in the surface layer compared to 0.9 eV in the bulk (10).

Figure 3 displays the reaction network to be assessed quantitatively in order to identify the reaction sequence with the highest overall rate. O_2 can be adsorbed on the perfect surface (top branch) or into a surface oxygen vacancy (bottom branch). Then the molecular adsorbates O_2^-, O_2^{2-} can dissociate either on the perfect surface (top branch) or

after incorporation into a surface oxygen vacancy (bottom branch). The final incorporation of O^- into a $V_O^{\cdot\cdot}$ after encounter of the two species is the same, independent of the starting point of the reaction.

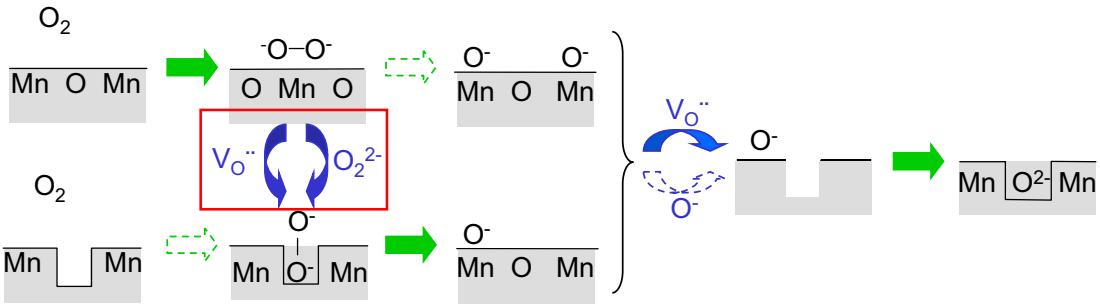

Figure 3. The most probable mechanism of oxygen incorporation on MnO_2[001]-terminated $La_{1-x}Sr_xMnO_{3\pm\delta}$ follows the solid arrows. Straight green arrows indicate reaction steps (chemisorption, dissociation, O^- incorporation), bent blue arrows describe transport (diffusion parallel to the surface). The rate-determining step (red frame) is the encounter of adsorbed molecular oxygen O_2^- or O_2^{2-} and a surface oxygen vacancy.

The first mechanism (M1) to be discussed begins with the adsorption of O_2 into a surface oxygen vacancy (bottom branch in Fig. 3). The rate is the product of the gas molecule impact rate ($8\cdot10^{-6}$ per surface unit cell and s), sticking coefficient (estimated to be 0.1) and surface vacancy concentration (10^{-4}), yielding 80 per surface unit cell and s. The "vertically adsorbed peroxide" thus formed is identical to the transition state shown in Fig. 1b. Its dissociation into a regular oxide ion occupying the vacancy and an O^- ontop of a Mn ion occurs fast and without barrier. In order to complete the oxygen incorporation this O^- has to meet another surface vacancy. As indicated in Fig. 1b, the diffusion of O^- along the surface has a high barrier of 2 eV. Thus it is the vacancy with the lower barrier of 0.67 eV that approaches the essentially immobile O^-. The respective rate is proportional to the concentration of O^- and of the surface vacancy as well as its diffusion coefficient $D_{V_O^{\cdot\cdot}}^{surf}$, and amounts to 10^6 per unit cell and s. The incorporation of O^- into a neighbouring $V_O^{\cdot\cdot}$ occurs fast and without barrier. Thus the first adsorption step is rate-determining for the overall process.

The alternative mechanism M2 (top branch in Fig. 3) starts with O_2 adsorption on the bare surface, which is exothermic by -1.1 eV as shown in Fig. 1a. Since no $V_O^{\cdot\cdot}$ is required here, the adsorption rate is high and amounts to $8\cdot10^5$ per surface unit cell and s. For the dissociation of the adsorbed O_2^- on the bare surface a barrier of 1.4 eV has been estimated preliminarily (14). Together with the O_2^- coverage this leads to a rate of 900 to $5\cdot10^4$ per unit cell and s. The subsequent encounter of the formed O^- and $V_O^{\cdot\cdot}$ is faster as shown for M1, thus the dissociation is rate-determining.

The final mechanism M3 under investigation also begins with O_2 adsorption on the bare surface. Instead of direct dissociation we now consider the encounter of O_2^- or O_2^{2-} and $V_O^{\cdot\cdot}$ as the next step (transition from top branch to bottom branch in Fig. 3). In contrast to M1 the coverage with molecular oxygen adsorbates is lower by about 1-3

orders of magnitude than for O^- (see Fig. 2), thus this rate amounts to 10^4 to $5 \cdot 10^5$ per surface unit cell and s. The incorporation of O_2^- or O_2^{2-} into the $V_O^{\cdot\cdot}$ after encounter occurs fast and without barrier, as well as the following dissociation. Since the approach of the resulting O^- and $V_O^{\cdot\cdot}$ occurs with a higher rate of 10^6 per surface unit cell and s (see M1 above), in M3 the O_2^{j-} - $V_O^{\cdot\cdot}$ encounter is rate-determining. The comparison with the other cases shows that M3 has the fastest rate of all discussed mechanisms. The variation of the different mechanisms' reaction rates with adsorbate coverage and surface oxygen vacancy concentration is displayed in Figure 4a. Depending on the actual concentrations of adsorbed O_2^- or O_2^{2-} and $V_O^{\cdot\cdot}$, the next faster mechanism is either M2 (high θ, low $[V_O^{\cdot\cdot}]$) or M1 (low θ, high $[V_O^{\cdot\cdot}]$). Additional details on the quantitative assessment of M1-M3 can be found in Ref. (9).

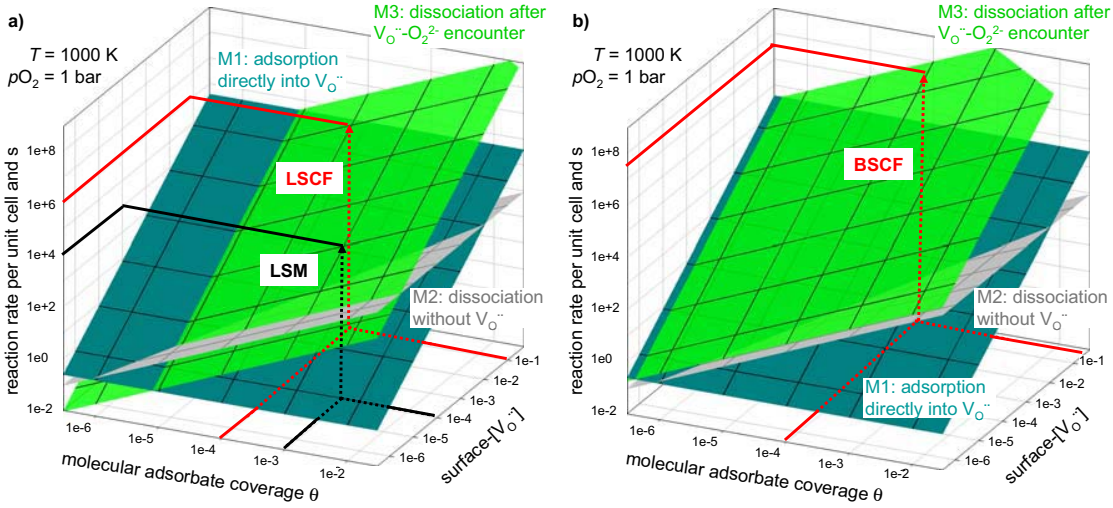

Figure 4. Variation of oxygen exchange rate on the TO_2[001] surface (T = transition metal) according to the different mechanisms M1-M3 with adsorbate coverage and surface oxygen vacancy concentration. a) (La,Sr)(Mn)$O_{3-\delta}$ (LSM) and (La,Sr)(Fe,Co)$O_{3-\delta}$ (LSCF) which have a comparable $V_O^{\cdot\cdot}$ mobility. b) The higher mobility of $V_O^{\cdot\cdot}$ in $Ba_{0.5}Sr_{0.5}Co_{0.8}Fe_{0.2}O_{3-\delta}$ (BSCF) (× 20 relative to LSCF (26)) selectively increases the rate for mechanism M3.

Based on the results for $La_{1-x}Sr_xMnO_{3\pm\delta}$, we can now "extrapolate" the kinetic considerations to the TO_2[001] terminated surface (T = transition metal) of other mixed conducting perovskites used as SOFC cathodes. For perovskites from the closely related (La,Sr)(Mn,Fe,Co)$O_{3-\delta}$ family, the bulk vacancy mobility and its activation energy (≈ 0.9 eV) is essentially independent of the actual cation composition (15,16) and a similar behaviour can be expected for the $V_O^{\cdot\cdot}$ surface mobility. The significant difference of the (La,Sr)(Mn)$O_{3-\delta}$ materials compared to (La,Sr)(Fe,Co)$O_{3-\delta}$ is their much less exothermic oxidation enthalpy ($\Delta H_{ox} = -\Delta H_{V_O^{\cdot\cdot}} \approx$ -3 eV per O for LSM, approx. -1 eV for LSCF (17-21)). This results in a much higher bulk vacancy concentration (e.g. $[V_O^{\cdot\cdot}] \approx 0.04$ for $La_{0.6}Sr_{0.4}Co_{0.8}Fe_{0.2}O_{3-\delta}$ (22)) and consequently also to a higher surface oxygen vacancy concentration. On the other hand the less exothermic oxidation enthalpy will also lead -

although to a smaller degree because less electrons are transferred in chemisorption than in complete oxygen incorporation - to a less exothermic adsorption enthalpy and consequently to lower oxygen adsorbate coverages. The barrier height for the rate-determining step of mechanism M3 is given by the barrier for $V_O^{\cdot\cdot}$ surface mobility. Since this barrier is comparable to that on LSM (see above), the reaction rates for LSCF materials can be represented by the same planes in Fig. 4a as for LSM. The consequence of the different defect and adsorbate concentrations for LSCF is shown in Figure 4a. The acceleration of the rate-determining step by the higher vacancy concentration dominates over the retardation due to the slightly lower adsorbate coverage. The rate of mechanism M1 is also increased by the higher $[V_O^{\cdot\cdot}]$ but still remains below that of M3. For mechanism M2 we assume that the barrier height for O_2^- dissociation will not change significantly since the lattice constants of LSM and LSCF are similar and thus also the geometry of the transition state can remain unaltered. Additionally, the higher vacancy concentration in LSCF increases the rate of M3 and M1 relative to M2 which thus becomes the slowest pathway. The resulting rate of M3 for LSCF is anticipated to be higher by about 2 orders of magnitude than for LSM, which is in excellent agreement with the oxygen exchange rates observed for those materials by microcontact impedance spectroscopy on dense thin-film electrodes (2,4). The experimental finding of a lower activation energy of the oxygen exchange rate for LSCF (approx. 1.3 eV (4, 23)) compared to LSM (approx. 2 eV (23,24)) is also in accord with the suggested mechanism M3, because the main contribution arises from the temperature dependence of $[V_O^{\cdot\cdot}]$, i.e. ΔH_{ox}.

Figure 4b displays the reaction rate for $Ba_{0.5}Sr_{0.5}Co_{0.8}Fe_{0.2}O_{3-\delta}$. In this cubic perovskite with a large bulk oxygen vacancy concentration (δ exceeding 0.5 without formation of superstructures such as brownmillerite (25)) oxygen vacancies are significantly more mobile than in the LSM and LSCF materials (26). This high mobility can be related to the presence of cations with lower charge (no La^{3+}; Co^{2+} instead of Fe^{3+} and Mn^{4+}) and high polarizability (Ba^{2+}, Co^{2+}) which also leads to a lower migration energy (0.5 eV instead of 0.8-0.9 eV for LSM and LSCF). While the experimental data refer to the bulk $V_O^{\cdot\cdot}$ mobility, a comparable relative increase is anticipated also for $V_O^{\cdot\cdot}$ moving parallel to the surface in the surface layer. As a consequence, the rate of mechanism M3 which involves the approach of $V_O^{\cdot\cdot}$ to adsorbed O_2^- or O_2^{2-} in the rate-determining step increases accordingly (27) and the corresponding plane in Fig. 4b is shifted to higher rates. The oxidation enthalpy of $Ba_{0.5}Sr_{0.5}Co_{0.8}Fe_{0.2}O_{3-\delta}$ is comparable to that of LSCF perovskites (28) thus adsorbate coverages are not expected to differ drastically (the more basic character of BSCF might slightly stabilize O_2^- or O_2^{2-} adsorbates). Mechanism M1 involves only the vacancy concentration and not their mobility, so it increases only slightly (29). A change in M2 barrier height is difficult to predict (the higher polarizability might lead to a certain lowering of the O_2^{2-} dissociation barrier, while the significantly larger lattice constant of should be unfavourable for transition state stabilization), nevertheless this mechanism so much slower that it cannot compete with M3 or M1 for BSCF materials. Therefore it is suggested that $Ba_{0.5}Sr_{0.5}Co_{0.8}Fe_{0.2}O_{3-\delta}$ also follows mechanism M3. Its rate is further accelerated relative to LSCF, again in good agreement with experiments (4).

Summary

Based on DFT calculations, a reaction mechanism for oxygen incorporation on the MnO_2[001] terminated surface of $La_{1-x}Sr_xMnO_{3\pm\delta}$ under SOFC operation conditions is proposed. In this mechanism the rate determining step comprises the encounter of molecular oxygen adsorbates O_2^- or O_2^{2-} and surface oxygen vacancies. This mechanism is expected to be valid not only for $La_{1-x}Sr_xMnO_{3\pm\delta}$ but for the entire (La,Sr)(Mn,Fe,Co)$O_{3-\delta}$ perovskite family. From the fact that the approach of a surface oxygen vacancy to adsorbed O_2^- or O_2^{2-} contributes significantly to the overall rate we can derive an optimization strategy for SOFC cathode materials keeping in mind that not only the surface vacancy concentration but also its mobility is crucial for fast oxygen exchange kinetics.

Acknowledgements

We thank U. Traub (MPI Stuttgart) for technical support, V. E. Alexandrov (MPI Stuttgart) and S. Piskunov (University of Essen) for valuable discussions. This work is supported in part by the National Science Foundation. Any appearance of findings, conclusions, or recommendations, expressed in this material are those of the authors and do not necessarily reflect views of NSF.

References

1. J. Mizusaki, T. Saito and H. Tagawa, *J. Electrochem. Soc.,* **143**, 3065 (1996).
2. J. Fleig, H.-R. Kim, J. Jamnik and J. Maier, *Fuel Cells,* **8**, 330 (2008).
3. J. Fleig, *J. Power Sources,* **105**, 128 (2002).
4. F. S. Baumann, J. Fleig, G. Cristiani, B. Stuhlhofer, H.-U. Habermeier and J. Maier, *J. Electrochem. Soc.,* **154**, B931 (2007).
5. G. Kresse and J. Furthmüller, *VASP the Guide*, Wien (2003**)**.
6. G. Henkelman, A. Arnaldsson and H. Jonsson, *Comp. Mater. Sci.,* **36**, 354 (2006).
7. R. A. Evarestov, E. A. Kotomin, Y. A. Mastrikov, D. Gryaznov, E. Heifets and J. Maier, *Phys. Rev. B,* **72**, 214411 (2005).
8. Y. A. Mastrikov, E. Heifets, E. A. Kotomin and J. Maier, *Surf. Sci.,* **603**, 326 (2009).
9. Y. A. Mastrikov, R. Merkle, E. Heifets, E. A. Kotomin and J. Maier, *submitted* (2009).
10. E. A. Kotomin, Y. A. Mastrikov, E. Heifets and J. Maier, *Phys. Chem. Chem. Phys.,* **10**, 4644 (2008).
11. S. Piskunov, Y. F. Zhukovskii, E. A. Kotomin, E. Heifets and D. E. Ellis, *MRS Symp. Proc.,* **894**, LL08-05 (2006).
12. J. Fleig, R. Merkle and J. Maier, *Phys. Chem. Chem. Phys.,* **9**, 2713 (2997).
13. [$V_O^{\ddot{}}$] estimated from D^* and $D_{V_O^{\ddot{}}}$ given in R. A. De Souza and J. A. Kilner, *Solid State Ionics,* **106**, 175 (1998).
14. Calculations for the dissociation transition state on the fully relaxed orthorhombic MnO_2[001] surface are in progress. Preliminary calculations for the transition state

on the cubic MnO_2[001] surface (with frozen lattice atom positions) yield a barrier height for the dissociation transition state of 1.4 eV relative to the tilted adsorbed superoxide O_2^-. In this transition state the molecular oxygen adsorbate is located on top of a surface oxygen ion such that the O-O bond is parallel to the Mn-O-Mn bonds in the surface layer. The O-O bond is elongated to 1.50 Å. Simultaneously the distance to the next surface Mn ions is already as short as Mn-O bulk distances which leads to a perceptible energy gain, but the Mn-O_{ad} bond is inclined by 52° relative to the surface plane.

15. J. A. Kilner, R. A. De Souza and I. C. Fullarton, *Solid State Ionics,* **86**, 703 (1996).
16. T. Ishigaki, T. Yamauchi, K. Kishio, J. Mizusaki and K. Fueki, *J. Solid State Chem.,* **73**, 179 (1988).
17. J. Nowotny and M. Rekas, *J. Am. Ceram. Soc.,* **81**, 67 (1998).
18. D. S. Mebane, Y. Liu and M. L. Liu, *Solid State Ionics,* **178**, 1950 (2008).
19. J. Mizusaki, M. Yoshihiro, S. Yamauchi and K. Fueki, *J. Solid State Chem.,* **58**, 257 (1985).
20. J. Mizusaki, Y. Mima, S. Yamauchi, K. Fueki and H. Tagawa, *J. Solid State Chem.,* **80**, 102 (1989).
21. R. Merkle, J. Maier and H. J. M. Bouwmeester, *Angew. Chemie Int. Ed.,* **43**, 5069 (2004).
22. K. Yasumoto, Y. Inagaki, M. Dokiya and T. Hashimoto, *Solid State Ionics* **159**, 71 (2003).
23. R. A. De Souza and J. A. Kilner, *Solid State Ionics,* **126**, 153 (1999).
24. G. J. la O', B. Yildiz, S. McEuen and Y. Shao-Horn, *J. Electrochem. Soc.,* **154**, B427 (2007).
25. S. McIntosh, J. F. Vente, W. G. Haije, D. H. A. Blank and H. J. M. Bouwmeester, *Solid State Ionics,* **177**, 1737 (2006).
26. L. Wang, R. Merkle, J. Maier, T. Acatürk and U. Starke, *Appl. Phys. Lett.,* **94**, 071908 (2008).
27. If for LSM and LSCF the mobilities of $V_O^{\cdot\cdot}$ and O_2^- or O_2^{2-} parallel to the surface contribute comparably to their encounter rate (9), then the higher $V_O^{\cdot\cdot}$ mobility for BSCF makes its contribution dominant and consequently also accelerates the overall rate.
28. L. Wang, R. Merkle, G. Cristiani, B. Stuhlhofer, H.-U. Habermeier and J. Maier, *ECS Transactions,* **13**, 85 (2008).
29. At first glance it may seem surprising that despite the high vacancy concentration the direct adsorption of O_2 into a surface vacancy (rate determining step of M1) is still slower than the encounter of O_2^- or O_2^{2-} and $V_O^{\cdot\cdot}$ (rate determining step of M3). However, the high vacancy concentration also accelerates the O_2^- or O_2^{2-} and $V_O^{\cdot\cdot}$ encounter (the average distance between adsorbates and $V_O^{\cdot\cdot}$ is only ≈ 5.7 Å, i.e. the length of two $V_O^{\cdot\cdot}$ jumps), and the additional increase of $V_O^{\cdot\cdot}$ mobility then results in M3 being faster than M1. A decrease of $D_{V_O^{\cdot\cdot}}^{surf}$ by one order of magnitude (or a significant increase of the adsorption sticking coefficient) would invert the relative sequence of reaction rates while still resulting in a high absolute rate.